J Appl Electrochem (2013) 43:53–63
DOI 10.1007/s10800-012-0504-3

ORIGINAL PAPER

Scratch resistance and electrochemical corrosion behavior of hydroxyapatite coatings on Ti_6Al_4V in simulated physiological media

T. Roland · H. Pelletier · J. Krier

Received: 17 July 2012 / Accepted: 29 October 2012 / Published online: 8 November 2012

Abstract Using an electrochemical process, needle-like hydroxyapatite crystals with Ca/P ratio of 1.67 were synthesized on Ti_6Al_4V without the formation of any precursor. In vitro dissolution/precipitation process was investigated by immersion of the coated substrate into Hank's solution up to 14 days. Physical and chemical characterizations were performed by scanning electron microscope coupled with energy dispersive X-ray spectroscopy and by X-ray diffraction. In particular, through a sequence of reactions including dissolution, precipitation, and ions exchange during immersion tests, a precipitated bone-like apatite coating homogenous and less porous was formed. Further, the corrosion behavior of the untreated and HA-coated specimens in simulated body fluid was evaluated using potentiodynamic polarization and electrochemical impedance spectroscopy. The results showed that the corrosion rates of the samples with HA layer before and after immersion tests were 72 and 80 % lower than that of the bare titanium alloy. At last, the adhesion of the HA layer was determined through the use of scratch tests. A particular tribological behavior and a strong link to the substrate were revealed.

T. Roland · H. Pelletier
Institut Charles Sadron, UPR22 CNRS, 22 rue de Loess, 67034 Strasbourg, France

T. Roland (✉)
INSA Strasbourg, 24 bld de la Victoire, 67084 Strasbourg, France
e-mail: thierry.roland@insa-strasbourg.fr

J. Krier
Laboratory of Surface Engineering of Strasbourg (LISS), 24 bld de la Victoire, 67084 Strasbourg, France

Keywords Biomaterials · Hydroxyapatite · Bioactivity · Corrosion · Adhesion

1 Introduction

Titanium and its alloys are widely used as implant materials in dental and orthopedic surgery due to their good biocompatibility with bone, owing to the presence of a very thin and native oxide film that spontaneously forms on the metal surface [1–3].

However, metallic surfaces are in general not sufficiently bioactive to chemically bond with the surrounding tissue which may lead to a weak fixation of the titanium [4–6]. Hence, surface treatment is usually needed to enhance the bioactivity so as to improve osseointegration with bone tissues.

In this way, titanium implants are commonly coated with hydroxyapatite (HA, $Ca_{10}(PO_4)_6(OH)_2$), a bioceramic that presents structural and chemical similarities to the mineral components of natural bones and teeth, so that surface bioactivity is enhanced. In fact, HA, characterized by a certain solubility, is gradually degraded and resorbed by the surrounding tissue which stimulates the bone growth on the material and through its pores, leading to a direct strong bond of the implants with the living bone [7]. In addition, the HA-coating may reduce the release of metallic ions from the implanted materials by acting as a barrier, that is not negligible when using Ti_6Al_4V. In fact, clinical studies have reported susceptibly to corrosive attack of Ti_6Al_4V by body fluids, with subsequent release of metallic ions that might cause local pain and swelling in the region of the implants and ultimately result in periprosthetic bone loss [8–11].

Hence, the enhancement of bioactivity and corrosion resistance of titanium implants has been the main research area in the recent years. Under this emulation, many coatings techniques have been developed such as plasma spraying [12], sol–gel [13], pulse laser deposition [14], electrophoretic deposition [15], and electrochemical deposition [16, 17].

The electrochemical (ECD) method introduced by Shirkhanzadeh [17], in the early 90's, has since gathered interest due to (a) the low temperatures involved (leading to low residual stress), (b) the ability to coat porous and irregular shape objects, and (c) the ability to control the thickness, composition, and microstructure of coatings. Depending on the electrolyte as well as the temperature used during the electrochemical process, different forms of calcium phosphates (Ca–P) can be obtained among which HA recognized as the most interesting form of calcium phosphates. Ban et al. [18] reported the formation of carbonate calcium phosphates of low crystallinity by an electrochemical method performed in a simulated body fluid electrolyte at 52 and 62 °C, whereas an amorphous phase was observed at 5, 22, and 37 °C.

Shirkhanzadeh demonstrated the formation of octacalcium phosphate (OCP)-type on cathodically polarized electrodes, using electrolyte containing dissolved calcium and phosphates ions at pH 4.4 [19]. Steam treatment followed by calcining at 425 °C or a post-treatment in alkaline solutions was necessary to convert these coatings into pure hydroxyapatite coatings. Redpenning et al. [20] also demonstrated that brushite ($CaHPO_4.2H_20$) was formed on titanium at room temperature from aqueous solutions saturated with $Ca(H_2PO_4)$, and that it may be converted into hydroxyapatite by treatment in alkaline solutions. Subsequent to this study, H. Benhayoune et al. [21] showed the possibility to convert the electrodeposited brushite coating into a stoichiometric hydroxyapatite through an hydrothermal treatment at 125 °C and pH 7 in an autoclave for 4 h and a calcining at 425 °C for 6 h. These selected studies illustrate the complexity in obtaining HA with a "simple process". However, it is also important to see the effects of electrodeposited HA-coatings on corrosion properties of the implant materials. In fact, the corrosion resistance of biomaterials is greatly affected by the presence of ceramic coatings as explained in [22, 23], both depending on the passivity ability of the metallic substrate and the porosity of the coating.

In this study, it is proven that with very low concentrations of calcium and phosphates ions and at pH 6.0, a pure hydroxyapatite layer can be deposited on cathodically polarized electrodes without the formation of a precursor phase.

In addition, studies were performed to assess the corrosion behavior of electrochemically HA-coated titanium alloys in Hank's solution using polarization and electrochemical impedance spectroscopy (EIS). At last, it is doubtful whether HA has enough stability in living body in the long-term when exposed to wear, chemical attack and to more load bearings during orthopedic applications. Therefore, the adhesion of the HA layer on Ti alloys was tested. Originality of this article comes from the fact that we developed a method to directly form a hydroxyapatite layer through an electrochemical process and without the need of subsequent operations. In addition, to the best of our knowledge, only few studies have so far concerned the scratch resistance of an electrochemically deposited hydroxyapatite layer on a titanium substrate.

2 Materials and methods

2.1 Electrochemical deposition: HA-coating

As-received commercial Ti_6Al_4V rod bar (Ø 20 mm) cut into disk of 2 mm thickness was used as the substrate. Before electrodeposition, the polished surface was pre-etched in sodium hydroxide (NaOH, 1 M) at 2 V for 10 min. to form specific surface structure favorable for apatite deposition. Electrodeposition was carried out for 3 h at 90 °C in a standard three-electrode cell, where platinum foil was used as anode and a saturated calomel electrode (SCE) was used as the reference electrode. The electrolyte used for the electrodeposition contained 0.61 mM $Ca(NO_3)_2$ and 0.36 mM $NH_4H_2PO_4$ prepared in deionized water, and its pH value was 6.2 just after preparation. A galvanostatic mode was used setting the current density to 1 mA cm^{-2} for 3 h. Stirring was carried out during the experiment. After deposition the specimens were rinsed in distilled water to remove residual electrolyte and dried in oven at 100 °C for 1 h.

2.2 Surface characterization

The crystallography of as-electrodeposited specimens was analyzed by grazing angle X-ray diffraction (GXRD-1°) using a Cu Kα radiation ($\lambda = 1.5418$ Å) and operated at a tube voltage of 40 kV and a current of 30 mA. The data was collected with a scanning rate of $1°min^{-1}$ in the 2θ range from 10 to 70°. The surface morphology and the chemical analysis of the coatings were observed by scanning electron microscopy combined with energy dispersive X-ray analysis (SEM/EDX, JEOL). Fourier transform infrared spectroscopy (FT-IR) was used to determine the vibration modes characteristic of the Ca–P coating.

2.3 Bioactivity tests

The in vitro bone bioactivity of the ceramic coatings was tested by examining their apatite forming ability by

soaking the samples in SBF Hank's solution (pH 7.4) at 37° ± 1 °C, according to the procedure reported by Kokubo and Takadama [24]. After 2 weeks, the samples were removed from the SBF solution, carefully rinsed with distilled water, and dried at room temperature for subsequent XRD and SEM analysis.

2.4 Corrosion measurements

Open circuit potential measurement (OCP) and cyclic potentiodynamic polarization of both coated and uncoated samples were carried out in Hank's physiologic solution (SBF-aqueous, 8 gL^{-1} NaCl, 0.4 gL^{-1} KCl, 0.14 gL^{-1} $CaCl_2$, 0.1 gL^{-1} $MgSO_4$, 0.06 gL^{-1} KH_2PO_4, 0.06 gL^{-1} Na_2HPO_4, 0.35 gL^{-1} $NaHCO_3$, 1 gL^{-1} glucose) at pH = 7.4 and T = 37 ± 1 °C, open to air. Corrosion tests were performed using a GAMRY potentiostat/galvanostat (model PC 5600-02034) with respect to the ASTM standard G61-94 [25]. All potentials were measured with respect to a saturated calomel electrode (SCE) as the reference electrode. A platinum electrode served as counter electrode for current measurement. First, the OCP was monitored as a function of time for 1 h, namely until a steady-state was reached. Next, cyclic potentiodynamic polarization measurement was performed from a potential of −1,000 to 4,000 mV versus SCE using a sweep rate of 1 mV s^{-1}. The sweep direction was then reversed when an anodic current density of 5 mA cm^{-2} was reached. Tafel extrapolation was used to determine the critical parameters such as the corrosion potential (E_{corr}) with the support of a commercial software. Electrochemical impedance spectroscopy experiments (EIS) were carried out in potentiostatic mode once the open circuit potential was established. The frequency range considered was from 100 kHz to 10 mHz, using a sinusoidal amplitude of ±10 mV for the perturbation signal. Data analysis was performed using a nonlinear least-squares fit method (developed by Boukamp [26]) to obtain the equivalent electrical model for the different substrate-electrolyte interfaces considered [27].

The impedance measurements were carried out before and after bioactivity tests.

2.5 Adhesion, scratch tests

The scratch test was conducted to evaluate the coating adhesion at the micro/macro-scales. Progressive load scratch test procedure was conducted using a Macro Revetest Scratch tester (CSM instruments) with a 200 μm tip radius rockwell diamond indenter. The diamond tip was drawn across the surface with a sliding speed of 10 mm min^{-1}, normal loads during ramp tests were increasing from 0.5 to 5 N.

3 Results and discussion

3.1 Surface characterization

The SEM micrograph of the electrodeposited coating shown in Fig. 1 indicated that the coating was composed of thin needle-like crystals with a length having an average value of 5 μm.

These elongated crystals were perpendicularly oriented to the surface and clearly formed a compact and uniform coating. From the GXRD analysis of these crystallites shown in Fig. 2a, the presence of a pure hydroxyapatite layer was revealed, as major peaks correspond to the (002), (210), (112), (202), and (213) reflection planes was assigned to hydroxyapatite using JCPDS file N°09-0432 (HA). A strongest reflection at 25.9° suggested a preferred orientation along the {002} planes. The high frequency of these planes may be related to the needle-like crystals strongly oriented along the

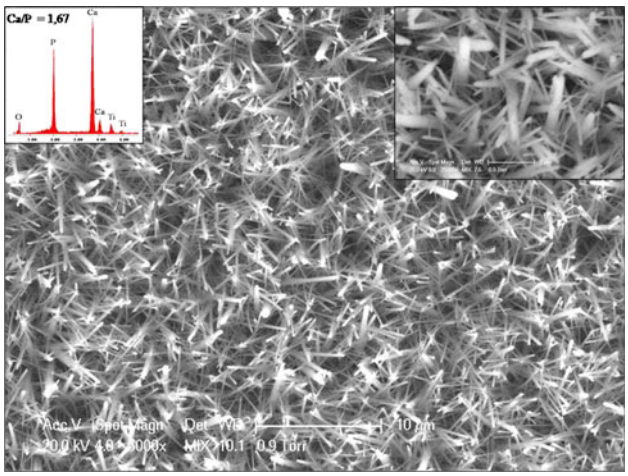

Fig. 1 Scanning electron micrograph of the calcium phosphate coating obtained by ECD and related EDX spectrum

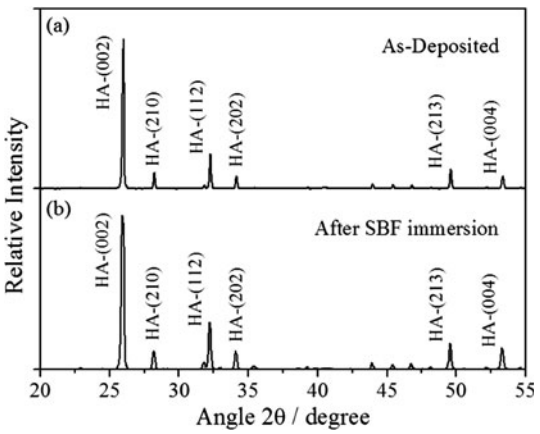

Fig. 2 X-ray diffraction spectra for the Ca–P coating (*a*) as prepared and (*b*) after 14 days of immersion in SBF

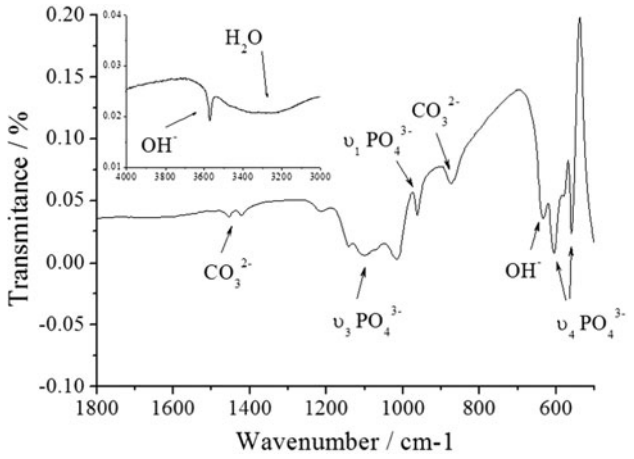

Fig. 3 FTIR spectra of the calcium phosphate coating prepared by ECD

c-axis as evident in Fig. 1. The sharp diffraction peaks also indicated that HA was well crystallized. DRIFT spectrum was also used to characterize the structure of the apatite formed layer (Fig. 3). According to this Fig. 3, all functional groups from HA were observed, here again, pointing out the presence of hydroxyapatite. First, a vibration band at 630 cm^{-1} was typical of structural OH^- in HA. A broadband in the region 3,000–3,600 cm^{-1} was assigned to stretching vibration of hydrogen bonded adsorbed water and hydroxyl ions, structural OH^- stretching peak at 3,570 cm^{-1} was typical of HA. A band in the region 950–980 cm^{-1} resulted from the υ1 symmetric stretching vibration of PO_4^{3-}. The band υ3 (asymmetric) of PO_4^{3-} had mostly been indexed in the range 1,040–1,125 cm^{-1}. At last, the prominent bands present in the ranges 550–600 cm^{-1} were characteristic of the anti-symmetric bending motion (υ4) of phosphate groups in hydroxyapatite. The presence of carbonate CO_3^{2-} at 865 cm^{-1} and at 1,400–1,450 cm^{-1} suggested carbonate ions substitution for either hydroxyl or the phosphate ions in HA during deposition as explained in [28]. From all these aspects, it can be concluded that under our electrodeposition conditions, hydroxyapatite may form directly on the cathode surface without the formation of a precursor phase such as OCP. In fact, the presence of OCP would be indicated by characteristics peaks of the bending mode of the HPO_4^{2-} group at 525 cm^{-1} and with the P–(OH) stretching mode around 860–915 cm^{-1}. A Ca/P ratio of 1.67 calculated from EDX also supposed the formation of a stoichiometric hydroxyapatite (Fig. 1). This could be of benefit in increasing the long-term durability of such coatings when applied in orthopedic implants since stoichiometric HA-coatings are more crystalline, and therefore less soluble in vitro and in vivo than other Ca–P coatings. All these observations were similar to previous findings [17, 29], in particular the preferred orientation of apatite coatings on titanium substrates had been reported before as being the result of a HA precipitation in two steps: an instantaneous nucleation (2D growth) and a progressive nucleation (3D growth).

3.2 Bone bioactivity

The bioactivity of HA-coated specimens was predicted examining the apatite formation on their surface in simulated body fluid. It should be pointed out that in the immersion test for bone bioactivity, the simulated body fluid used in the present study did not contain any biological matter such as bone-forming cells. Nevertheless, it has been pointed out in a recent review by Kokubo and Takadama [24] that results of immersion tests in inorganic simulated body fluids (of which Hank's solution) were useful in predicting in vivo bone bioactivity.

After immersion in Hank's solution for 14 days, the coating underwent a significant change in morphology as illustrated with the Fig. 4. From this figure, thick needle shape crystallites of higher diameter size compared to the as deposited condition (Fig. 1) were observed. In addition, apatite spherules of about 2–3 μm diameters seemed to have precipitated forming aggregates distributed over the surface (see inset, Fig. 4). The phase composition of these precipitates was identified as hydroxyapatite, as shown by the XRD spectra in Fig. 2b. It could be observed that the intensity of the apatite peaks has increased significantly, indicating that apatite was grown on the specimen after immersion in SBF from the previously formed HA layer.

The dissolution/precipitation process of the coating was also explored across the pH and weight variation of the Hank's solution and of the coating, respectively (Figs. 5, 6). From these figures, it is clear that apatite was newly formed through a sequence of reactions including dissolution, precipitation, and ions exchange. The initial increase in pH value observed in Fig. 5 may be a result of the dissolution of HA that release OH^- into the solution. After few days of

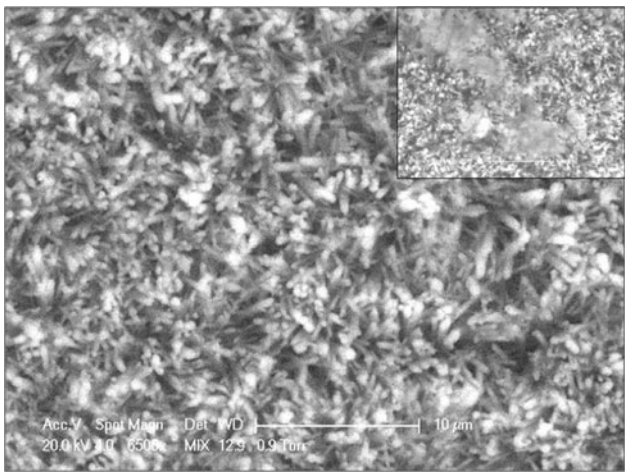

Fig. 4 SEM micrographs of HA after 14 days of immersion in SBF

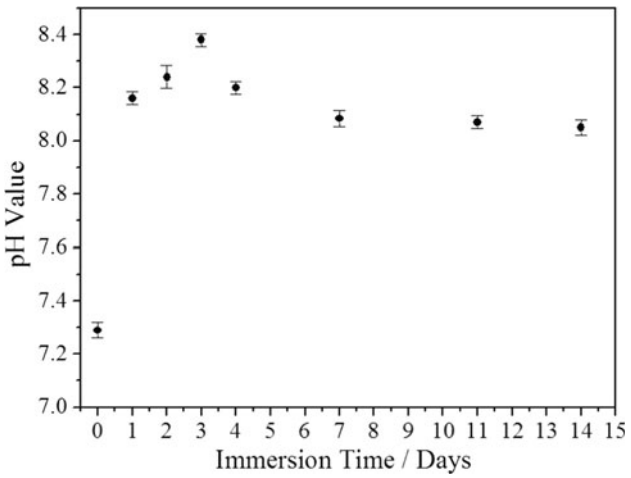

Fig. 5 pH value variation during immersion

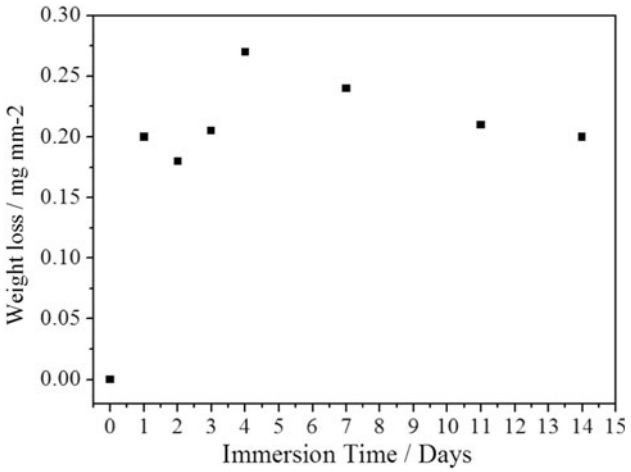

Fig. 6 Weight loss variation of HA coating during immersion

immersion, the pH value reached a maximum (between 8 and 8.5) then decreased with immersion time. This decrease in the pH value could be explained by the above-mentioned precipitation of the apatite, which consumes OH^- and/or HPO_4^{2-} in the solution. The weight losses (mg mm^{-2}), shown in Fig. 6, was consistent with the pH values results, and thus first increased (dissolution) and then reached a maximum value to finally decreased (precipitation). All these aspects are in accordance with the chemical model for the dissolution of the calcium phosphates proposed in [30, 31]. The initial stages of dissolution of apatite consist of calcium detachment from the surface. When all neighboring cations of calcium (Ca^{2+}) have been removed, phosphates groups (PO_4^{3-}) also detach from the surface increasing the ions concentrations in the solution up to a supersaturated state that leads to a re-precipitation of apatite. This model is particularly adapted to our specimens since the EDS semi-quantitative analysis has revealed a value of 1.67 for the Ca/P ratio, and that it has been proven that the model is particularly relevant and observed for coatings near the stoichiometric value (more precisely with Ca/P ratio higher than 1.6) as explained in [30].

This crystal growth behavior in SBF may be explained by the supersaturation solution effect that happens before re-precipitation. As mentioned in [32], it may be assumed that under immersion, the driving force that governs the morphology change is the degree of supersaturation in the vicinity around the tips of the HA crystals. In case of low degree of supersaturation, it is well-known that crystals may grow due to spiral growth theory [33]. With the precipitation process going, the degree of supersaturation around the tips of the HA crystal comes down: the pH value around the tips decreases accompanied with a reduction of the CaP salts solubility [34]. Thus, HA crystals may grow accordingly to the spiral growth theory, leading to hexagonal spirals on the tips with a size expansion of the needle shape rods as observed in Fig. 4. It would be premature to make the shortcut that the precipitation process observed here is the same as in vivo.

In addition, compared to the HA crystals in the as deposited state, after immersion HA crystals became larger in dimension, not only regarding the average diameter but also regarding the longitudinal length. We assumed that a low pH value in the vicinity of the HA crystals, during precipitation, is responsible for this. It has been demonstrated that average longitudinal length of HA crystals prepared electrochemically under higher pH value was shorter than the ones prepared under lower values [32].

3.3 Electrochemical characterization

3.3.1 Open circuit potential (OCP) measurement

Figure 7 shows the variation in the potential with time between the native titanium oxide film (AR-Ti_6Al_4V), the

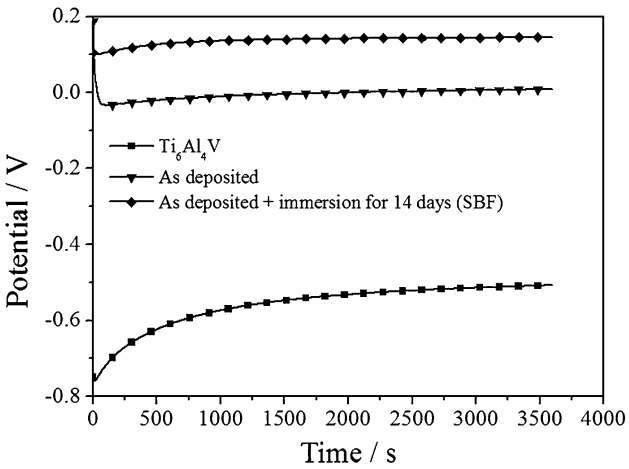

Fig. 7 Plot of open circuit potential versus time for as-received titanium, for HA-coated and for HA-coated with 14 days immersion in SBF samples

HA-coated and the HA-coated after immersion-bioactivity test specimens in Hank's solution at 37 °C.

It was observed that OCP of untreated titanium alloys was around −0.55 V, while the HA-coated titanium were all nobler, showing higher thermodynamic stability.

This indicated the protective nature of the coatings. The noble behavior of the HA coatings could be due to the insulating nature of the surface [35]. However, the HA coatings obtained were microporous in nature (because of the reduction of water that occurred at the cathode leading to the formation of H_2 bubbles), and hence the electrolyte streamed into the coating through the pores. Thus, the OCP-time behavior of HA-coated samples after 14 days immersion in SBF showed a little increment on values of E_{OCP} due to the precipitations from physiological solutions that sealed the pores left by the ceramic coating.

This proves that the deposited coating has a protective character that increases with the immersion time in SBF and once precipitation is reached.

3.3.2 Potentiodynamic polarization studies

The potentiodynamic polarization studies were carried out for the as-received Ti_6Al_4V and HA-coated Ti_6Al_4V specimens, in the as deposited state and after additional immersion for 14 days in SBF. The results are presented in Fig. 8. All the specimens were spontaneously passive upon anodic polarization and none of the polarization curves exhibited hysteresis loop, indicating the absence of passivity breakdown. Compared with bare samples, the alloy covered with HA followed or not by immersion in SBF exhibited an improvement in corrosion resistance as indicated by lower anodic current densities.

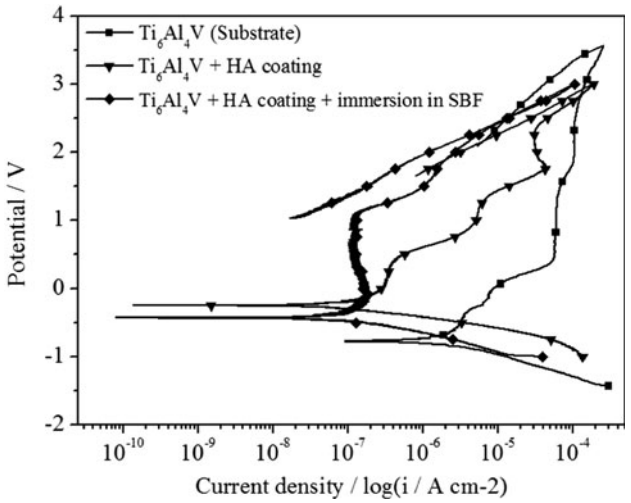

Fig. 8 Potentiodynamic polarization curves of the native titanium oxide film, the HA-coating and the HA-coating after immersion in SBF for 14 days

Table 1 Corrosion parameters for various samples (Uncoated/HA-coated) in Hank's solution

Sample	E_{corr} (mV)	I_{corr} (μA cm^{-2})	Corrosion rate (mm year^{-1})
As-polished	−773	2.32	0.095
HA-coated	−434	0.188	0.027
HA + immersion SBF	−231	0.136	0.019

The corrosion current density I_{corr}, corrosion potential E_{corr}, and corrosion rate were calculated using tafel extrapolation and are presented in Table 1. All electrochemical parameters (Table 1) had more favorable values for coated materials.

Corrosion potential (E_{corr}) exhibited more electropositive values for the coated materials than for the uncoated, confirming the beneficial influence of the coating.

The alloy covered with HA and immersed in SBF showed an increase protective character against corrosion, in comparison to the only HA-coated samples, as indicated by the lower corrosion rate. It is generally admitted that the HA layer acts as a barrier to the transport of electrons and ions between the substrate and the electrolyte, thus reducing the electrochemical reaction rate, as demonstrated here. When pores are present in the HA coating, conducting paths between the corrosive medium and the metallic substrate will eventually be formed leading to preferential sites of corrosion [36, 37]. The shift in current density to lower values for the HA-coated-immersed samples can thus be explained by the formation of a denser and less porous HA coating in consequence of precipitated compounds from SBF reducing the layer defects [38].

3.3.3 Electrochemical impedance spectroscopy (EIS)

Figures 9 and 10 show the Nyquist and Bode diagrams, respectively, for the bare and HA-coated Ti_6Al_4V with or without an additional 14 days of immersion in physiological solution.

Nyquist spectra (Fig. 9) revealed incomplete semicircles with very large radius of curvature that show a capacitive behavior, suggesting a very protective passive layer. The impedance values for the coated samples were higher than those for the uncoated substrate, which proves a nobler electrochemical behavior of the deposited coatings that impede the ion diffusion process and reduce the corrosion rate of the substrate.

Also, the impedance of the coated materials increased after the immersion period suggesting a thicker or more compact coating as a result of the observed hydroxyapatite deposition.

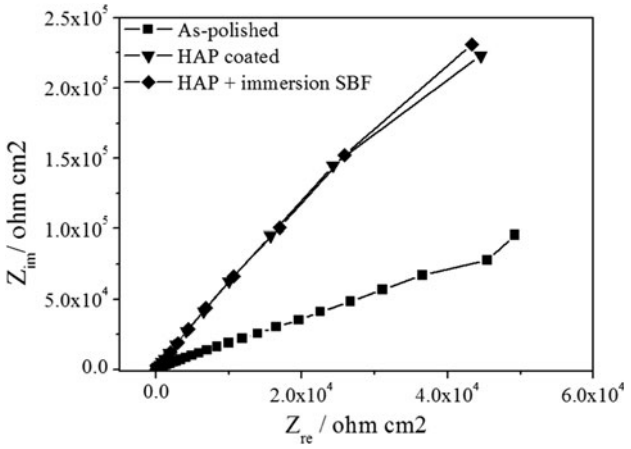

Fig. 9 Nyquist plot in Hank's solution for uncoated, HA-coated and HA-coated with immersion in SBF samples

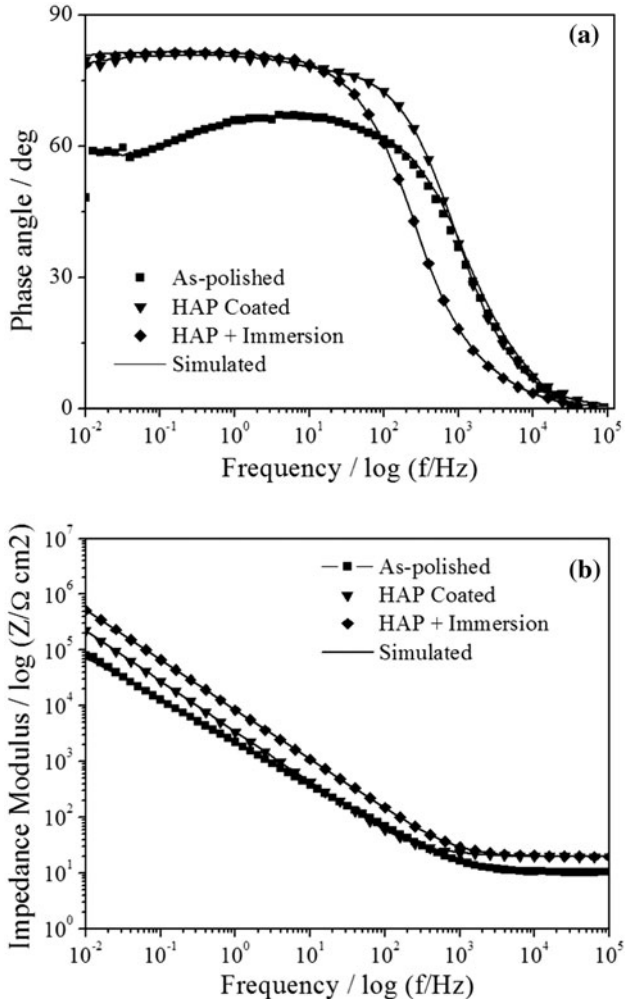

Fig. 10 Impedance spectrum of as-received titanium alloy, as HA-coated and as HA-coated with immersion test samples in the form of **a** bode phase-angle plot and **b** bode- impedance plot

Since Nyquist plots are relatively featureless, the Bode plots, known to be more indicated for the investigation of changes in the electrochemical characteristics of a system, were used.

For the interpretation of the electrochemical behavior of a system from EIS spectra, an appropriate physical model of the electrochemical reactions occurring on the electrodes was necessary. After testing a number of different electrical circuit models for the analysis of the obtained impedance spectra (Figs. 9, 10), it was found that the whole set of data could be satisfactorily fitted with the equivalent circuits given in Fig. 11. It was based on the consideration of a two-layer model for the surface film. It consisted of the following elements: a solution resistance R_e of the test electrolyte, electrical leads, etc., the capacitance C_p of the coating layer, the charge transfer resistance associated with the penetration of the electrolyte through the pores or pinholes existing in the coating R_p; and the polarization resistance of the susbstrate R_b as well as the electrical double-layer capacitance at the substrate/electrolyte interface C_b. A constant-phase element (CPE) representing a shift from an ideal capacitor was used instead of the capacitance itself due to the almost complete absence of pure capacitance in the real electrochemical process. The impedance representation of CPE was given by:

$$Z_{CPE} = 1/[Q(jw)^n] \quad (1)$$

where w is the angular frequency and n related to the non-equilibrium current distribution due to the surface roughness and surface defects.

Fitting parameters obtained from adjustment using ZView software are presented on Table 2. The agreement between experimental and simulated results indicated a good fitting.

According to literature [39–41] the film on Ti alloys is composed of a bi-layered oxide consisting of a porous outer layer and a barrier inner layer. In work performed by Lavos-Valereto et al. [41] with Ti_6Al_7Nb alloy, in Hank's solution, two relaxation time constants were clearly indicated by two peaks on phase-angle plots. Based on these facts the selected "equivalent circuit" as shown in Fig. 11 was rather pertinent. Similar fittings were previously found by Pan et al. [42] for titanium immersed in saline solution, which emphasizes the duplex nature of the passive film.

A highly capacitive behavior, typical of passive materials, was indicated from medium to low frequencies by phase angles approaching $-70°$ up to $-90°$, suggesting that a highly stable film was formed on all tested alloys in the electrolyte used. This is consistent with the very low corrosion rates determined in polarization tests (Table 1). R_b was significantly larger than the values associated to the outer porous layer, R_p as shown in Table 2. These results indicated that the protection provided by the passive layer

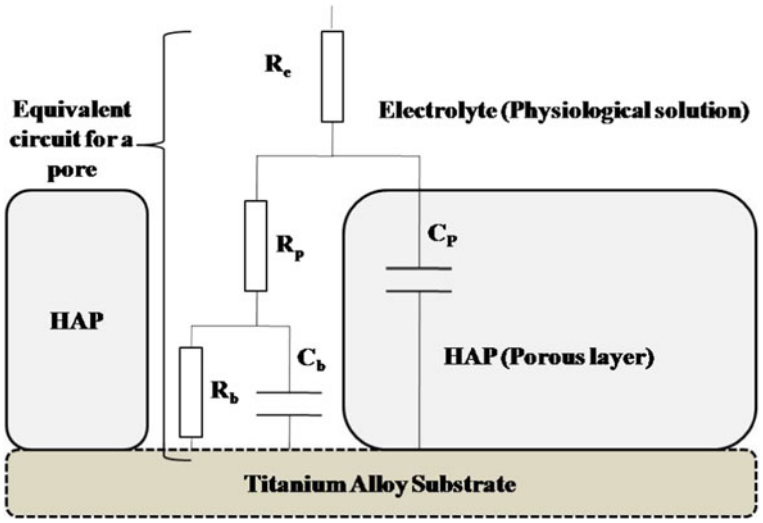

Fig. 11 Equivalent circuit used for fitting experimental parameters. Symbols are explained in the text

Table 2 EIS fitting parameters for the untreated titanium alloy and HA-coated samples with and without immersion in SBF for 14 days

Surface type	R_S (Ω)	Q_P (F cm^{-2})	$n(Q_P)$	R_P (Ω cm^{-2})	Q_b (F cm^{-2})	$n(Q_b)$	R_P (Ω cm^{-2})
As-polished	10.21	7.54×10^{-5}	0.81	98.67	2.99×10^{-5}	0.72	2.18×10^{5}
HA-coated	19.8	2.25×10^{-5}	0.89	147.9	7.54×10^{-5}	0.98	2.92×10^{6}
HA + immersion	19.67	3.39×10^{-5}	0.90	957	2.07×10^{-5}	0.90	1.59×10^{7}

is predominantly due to the barrier layer. It could also be observed some marginal changes in the values of the solution resistance (R_s) after immersion period. This can be associated with the change in the ionic strength of the solution with time in relation to precipitation process (adsorption of solution ions).

Bode-impedance plots (Fig. 10b) were characterized by two distinct regions: first in the higher frequency region due to the response of the electrolyte resistance and second in the low and middle frequency range due to the response of the capacitive behavior of the surface film.

An increase of R_p was observed after immersion period for the HA-coated samples, as a result of a progressive blocking effect due to Ca–P precipitation inside the pores in the ceramic coating.

In addition, no significant change of the Q_p and Q_b values was observed and low values of n indicated a rough surface for coated samples. All these aspects support the idea that variations in the electrochemical process after immersing period were essentially due to changes in the chemical environment inside the pores of the HA layer.

Regarding the values of R_p and R_b that were much higher for the HA-coated samples than those determined for the bare sample, it may be concluded that HA hindered the electrochemical process occurring at the metal substrate interface thus leading to a decrease in the metal ion release from the alloy. R_p increased slightly after immersion time, which indicates that the pores were probably filled with the precipitated products from the solution.

According to [43], covered area with HA may be calculated using equation:

$$1 - \theta = \frac{R_{to}}{R_t} \tag{2}$$

where θ is the coverage area, R_t is the charge transfer resistance of the HA-deposited Ti alloy, and R_{to} is the resistance of native oxide film on Ti alloy. Because the HA layer is a non-conductive layer and thus assuming that current can only pass at bare spots, Eq. 2 can be applied [43]. The coverage of titanium surface after electrochemically HA deposit was 92.6 %, whereas after HA-coating

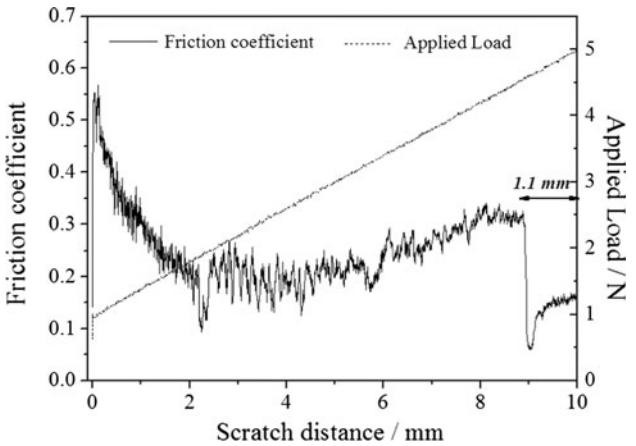

Fig. 12 Friction and Load versus distance curve of HA-coated specimen for scratch test

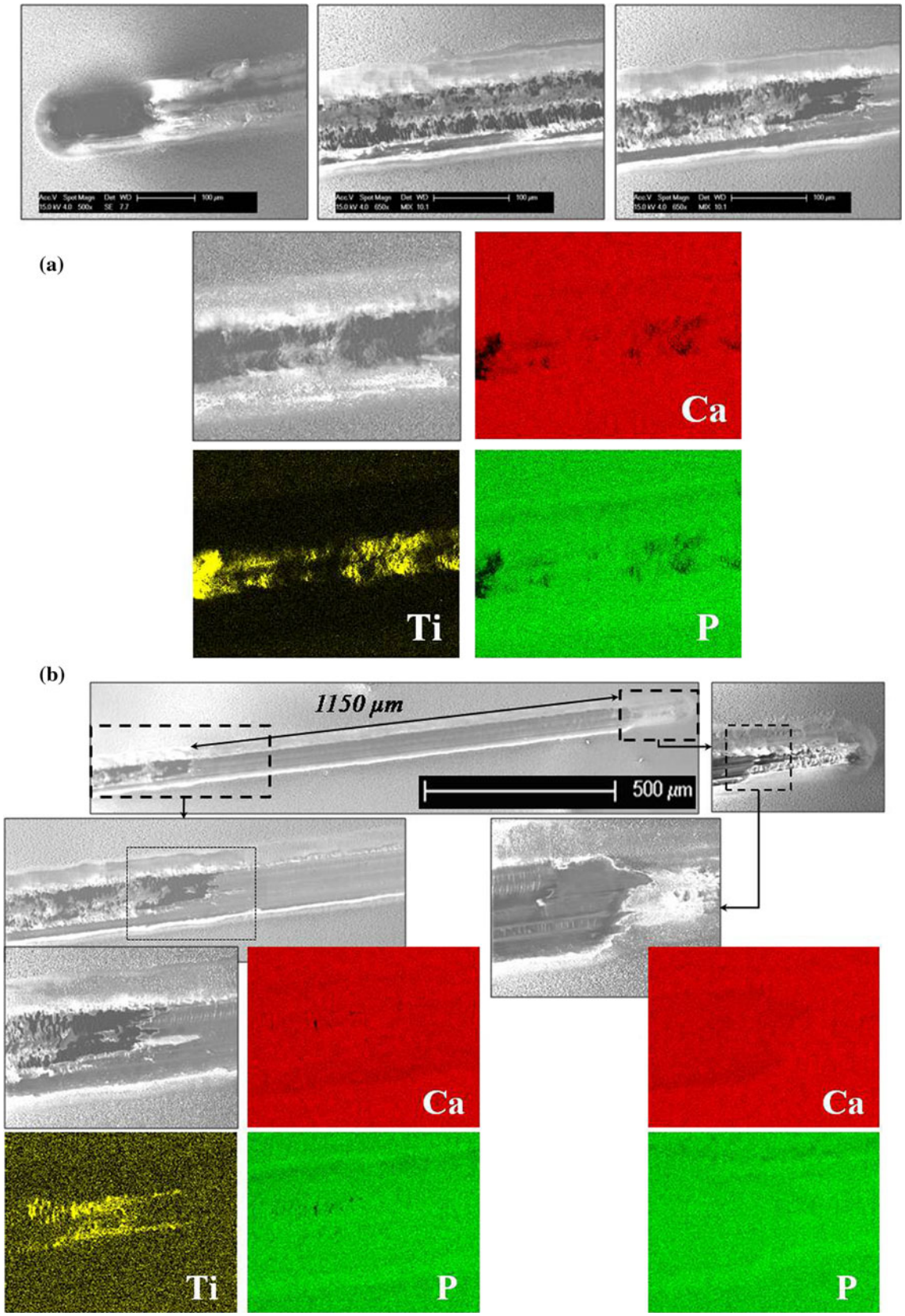

Fig. 13 SEM/EDX photographs of the scratch track **a** at the beginning of the scratch and **b** close to the end of the scratch

and immersion period, this value went to 98 %, which tend to prove that precipitation process had effectively played an interesting role in increasing the corrosion resistance of the substrate Ti alloy.

3.4 Scratch resistance

Based on [16, 21], a chemical link was established between the HA layer and the substrate through the electrochemical process, with possible water reduction at the cathode depending on the current density. This aspect may cause H_2 bubbles at the cathode leading to poor adhesion of the HA layer.

Figure 12 shows the friction/load-distance curve of the HA-deposited specimen, whereas SEM picture of the scratch track is shown on Fig. 13 with the associated EDX analyses. Experimental results indicated that the HA coating was not scrapped off by diamond indenter, and more remarkably, more greater was the applied load and more adherent was the coating, as revealed by the Fig. 13a. In fact, at the beginning of the scratch and thus under low loads (<2 N), some detachments of the coating might be observed, whereas after exceeding a certain load (above 2 N), any scrap off was observed. Due to the porous morphology of the HA layer prepared by ECD, the damage was mainly restrained within the coating and only in the contact area, without any delamination phenomenon. This behavior is quite different from those observed for Ca–P coatings prepared by plasma spray [44]. It may be qualified of a rigid-plastic behavior as a snow-like, and the sudden decrease of the friction coefficient at about 1.1 mm of the end of the scratch was due to the flattening of the coating leading to a smooth and sliding surface as particularly shown on Fig. 13b, where the region is revealed in the SEM/EDX pictures.

4 Conclusion

From these studies, it can be inferred that ECD process is a promising method to perform HA layer on titanium surface and especially with a biomimetic morphology which is a positive parameter in coated implant lifetime.

The in vitro apatite formation during exposure to SBF, generally accepted as indicator for in vivo bone bioactivity of the material surface, has shown good results of the electrochemically deposited HA. After immersion in SBF, hexagonal rod-like HA crystals of higher cross section diameter in comparison to those obtained in the as deposited state were produced through a sequence of reactions including dissolution, precipitation, and ions exchanges. Regarding our experimental conditions with a relatively low supersaturation process once the precipitation process was nucleated, the spiral growth model introduced by the Burton-Canberra-Franck theory was found to better interpret the precipitated coating morphology.

The hydroxyapatite coating was revealed as playing the role of a protective layer between the metallic substrate and biological environment and thus increased the corrosion resistance of the implant material. The EIS spectra demonstrated an evolution with elapsed time that reflects that the pores in the coatings were progressively filled with precipitates leading to high value of R_p.

At last, from scratch tests, it was demonstrated that the HA coating was well adherent to the substrate and that damages were limited to the scratch tip area.

Acknowledgments The authors gratefully acknowledge the institute IS2 M of Mulhouse for the assistance in obtaining the DRIFT spectra presented in Fig. 3.

References

1. Leitao E, Silva RA, Barbosa MA (1997) Corros Sci 39:333
2. Breme HJ, Helsen JA (1998) In: Helsen JA, Breme HJ (eds) Metals as biomaterials. Wiley, Chichester, pp 1–35
3. Elagli K, Traisnel M, Hildebrand HF (1993) Electrochim Acta 38:1769
4. Calson SL, Rostlunt TR, Abrektsson B, Abrektsson T, Branemark PL (1986) Acta Orthop Scand 57:285
5. Bardson DI (1990) In: William D (ed) Encyclopedia of medical and dental materials. Pergamon, Oxford, p 360
6. Kasemo B (1983) J Prosthet Dent 49:832
7. Schouten C, Meijer GJ, Van den Beucken JJJP, Leeuwenburgh SCG, De Jonge LT, Wolke JGC (2010) Acta Biomater 6:2227
8. Hallab NJ, Mikecz K, Vermes C, Skipor A, Jacobs JJ (2001) J Biomed Mater Res 56:427
9. Shirkhanzadeh M (1992) J Mater Sci Mater Med 3:322
10. Park JB, Lakes RS (1992) Biomaterials—an introduction. Plenum, New York, pp 75–115
11. Urban RM, Jacobs JJ, Gilbert JL, Galante JO (1994) J Bone Joint Surg 76A:1345
12. Chen CC, Huang TH, Kao CT, Ding SJ (2006) J Biomed Mater Res B Appl Biomater 78B:146
13. Wang D, Chen C, He T, Lei T (2008) J Mater Sci Mater Med 19:2281
14. Dinda GP, Shin J, Mazumder J (2009) Acta Biomater 5:1821
15. Kwok CT, Wong PK, Cheng FT, Man HC (2009) Appl Surf Sci 255:6736
16. Eliaz N, Eliyahu M (2007) J Biomed Mater Res A 80:621
17. Shirkhanzadeh M (1991) J Mater Sci Lett 10:1415
18. Ban S, Maruno S (1995) Biomaterials 16:977
19. Shirkhanzadeh M (1994) Nanostruct Mater 4:677
20. Redpenning J, Schlessinger T, Burnham S, Lippielo L, Miyano J (1996) J Biomed Mater Res 30:287
21. Benhayoune H, Laquerriere P, Jallot E, Perchet A, Kilian L, Balossier G et al (2002) J Mater Sci Mater Med 13:1057
22. Gross KA, Berndt CC (1994) J Mater Sci Mater Med 5:219
23. Sousa SR, Barbosa MA (1995) J Mater Sci Mater Med 6:818
24. Kokubo T, Takadama H (2006) Biomaterials 27:2907
25. ASTM Standard, G61-86, Conducting cyclic potentiodynamic polarization measurements for localized corrosion susceptibility in iron-, nickel-, or cobalt-based alloys, ASTM Standards, ASTM
26. Boukamp BA (1986) Solid State Ion 20:31

27. Brett CMA, Brett AMO (1998) Electrochemistry: principles, methods and application. Oxford University Press, Oxford
28. LeGeros RZ (1994) In: Brown PW, Constantz B (eds) Hydroxyapatite and related materials. CRC, FL, pp 3–28
29. Vijayaraghavan TV, Benesalem A (1994) J Mater Sci Lett 13:1782
30. Dorozhkin SV (2002) Prog Cryst Growth Charact 44:45
31. Zhang Q, Chen J, Feng J, Cao Y, Deng C, Zhang X (2003) Biomaterials 24:4741
32. Ma M, Ye W, Wang XX (2008) Mater Lett 62:3875
33. Verma A (1951) Nature 167:939
34. Ban S, Hasegawa J (2002) Biomaterials 23:2965
35. Vasilescu C, Drob P, Vasilescu E, Demetrescu I, Ionita D, Prodana M, Drob SI (2011) Corros Sci 53:992
36. Narayanan R, Seshadri SK (2008) Corros Sci 50:1521
37. Zhang Z, Dunn MF, Xiao TD, Tomsia AP, Saiz E 2002 Nanostructured hydroxyapatite coatings for improved adhesion and corrosion resistance for medical implants. Nanotech & Biotech Convergence-2002, Stamford, pp. 291–296
38. Mondragon-Cortez P, Vargas-Gutierrez G (2004) Mater Lett 58:1336
39. Souto MR, Laz MM, Reis RL (2003) Biomaterials 24:4213
40. Venugopalan R, Wiemer JJ, George MA, Lucas LC (2000) Biomaterials 21:1669
41. Lavos-Valereto IC, Wolynec S, Ramires I, Guastaldi AC, Costa I (2004) J Mater Sci Mater Med 15(1):55–59
42. Pan J, Thierry D, Leygraf C (1996) Electrochem Acta 41:1143
43. Sabatani E, Cohen JB, Bruening M, Rubinstein I (1993) Langmuir 9:2974
44. Chern Lin JH, Lin HJ, Ding SJ, Ju CP (2000) Mater Chem Phys 64:229